

# Vertical Addressing of 1-Plane Electrodes for Digital Microfluidics

Sebastian von der Ecken, Alexandros A. Sklavounos, and Aaron R. Wheeler\*

Digital microfluidics (DMF) has become a mainstay in the microfluidics and microelectromechanical communities. Many users rely on simple DMF devices featuring a small number of rows and columns of electrodes that can be rapidly manufactured using “one plane” lithographic or printing techniques. But as the popularity of DMF grows, there are increasing needs for larger devices that can facilitate multiplexed handling of many samples and reagents in parallel. One option for scaling DMF devices is to use “vertical addressing” techniques such as printed circuit boards (PCBs), but PCBs formed using standard techniques exhibit topography that is not ideal for smooth and reliable droplet movement. A new method to produce DMF devices using vertical addressing of 1-plane electrodes (VAPE-DMF) is introduced. This method, which separates devices into “covers” (bearing 1-plane electrodes) and “sub-substrates” (for vertical addressing), enables rapid and inexpensive manufacture of devices with arbitrarily large driving electrode arrays. This work describes how to manufacture VAPE-DMF devices and demonstrates a proof-of-concept device with an array of 336 electrodes to handle 48 droplets to run 24 reactions in parallel. It is proposed that VAPE-DMF represents a useful new development for the growing community of users and innovators of digital microfluidics and related methods.

for droplet actuation in digital microfluidics is often described in terms of “electrowetting on dielectric” (EWOD).<sup>[5]</sup> In this scheme (Figure 1a), when a voltage is applied between a driving electrode and the ground-electrode, droplets adjacent to the driving electrode experience an electrostatic force  $F_{EWOD}$ . If  $F_{EWOD}$  is greater than a resistive force  $F_{Resist}$  (which can include contact-line pinning, viscous drag, and viscous dissipation, among others<sup>[6]</sup>), the droplet moves onto the activated electrode (Figure 1a). Similarly, simultaneous actuation of electrodes on opposite sides of a droplet can cause it to split into two or more sub-droplets, which forms the basis for a “dispense” operation. Thus, DMF offers the ability to automatically move, dispense, merge, and mix droplets of different reagents on a lab-on-a-chip, similar to a technician pipetting reagents into wells of a microtiter plate. Analogously, the greater the density of driving electrodes (for DMF) or wells (for microtiter plates), the more useful the system is for multiplexed/parallel operations and analyses.


## 1. Introduction

Digital microfluidics (DMF) is a versatile technique in which droplets of reagents are manipulated on the surface of an insulated, hydrophobic array of driving electrodes. DMF is commonly implemented in a two-plate format in which the driving electrodes are on a bottom plate and a counter electrode is on a top plate, with droplets sandwiched between them.<sup>[1–4]</sup> The functional principle

The driving electrode arrays that are used in DMF bottom plates are typically laid out as a two-dimensional grid. Electrode dimensions are commonly 0.5–2.5 mm per side, and each electrode is typically separated from its adjacent neighbors by tens of micrometers. Each driving electrode is (typically) individually addressable—using a 20–100 micrometer wide conductive trace to connect each driving electrode to a dedicated contact pad at the edge of the bottom plate. The contact pad allows the device to interface with the DMF control system which can apply an electric potential to each pad independently, and by extension each electrode. The methods used to fabricate driving electrode arrays on the bottom plates of DMF devices can be roughly categorized as either “1-plane-electrode” techniques or “vertical addressing” techniques. (Note that the phrase “coplanar electrodes” is often used to describe “single plate” DMF devices. Here, we are focused on the more common “two plate” device format, and thus use an alternate term, “1-plane-electrodes” to try to emphasize the difference.) In devices formed by 1-plane-electrode techniques (Figure 1b), all of the electrical architecture (the driving electrodes, the electrically conductive traces, and the contact pads) are formed on the same plane of the bottom plate. In devices formed by vertical addressing techniques (Figure 1c), the DMF driving electrode array is on a single plane, but the conductive traces that connect to the driving electrodes are formed vertically, allowing for electrical

S. von der Ecken, A. A. Sklavounos, A. R. Wheeler  
Department of Chemistry  
University of Toronto  
80. St. George Street, Toronto, Ontario M5S 3H6, Canada  
E-mail: aaron.wheeler@utoronto.ca

A. A. Sklavounos, A. R. Wheeler  
Donnelly Centre for Cellular and Biomolecular Research  
University of Toronto  
160 College Street, Toronto, Ontario M5S 3E1, Canada  
A. R. Wheeler  
Institute of Biomedical Engineering  
University of Toronto  
164 College Street, Toronto, Ontario M5S 3G9, Canada

 The ORCID identification number(s) for the author(s) of this article can be found under <https://doi.org/10.1002/admt.202101251>.

DOI: 10.1002/admt.202101251

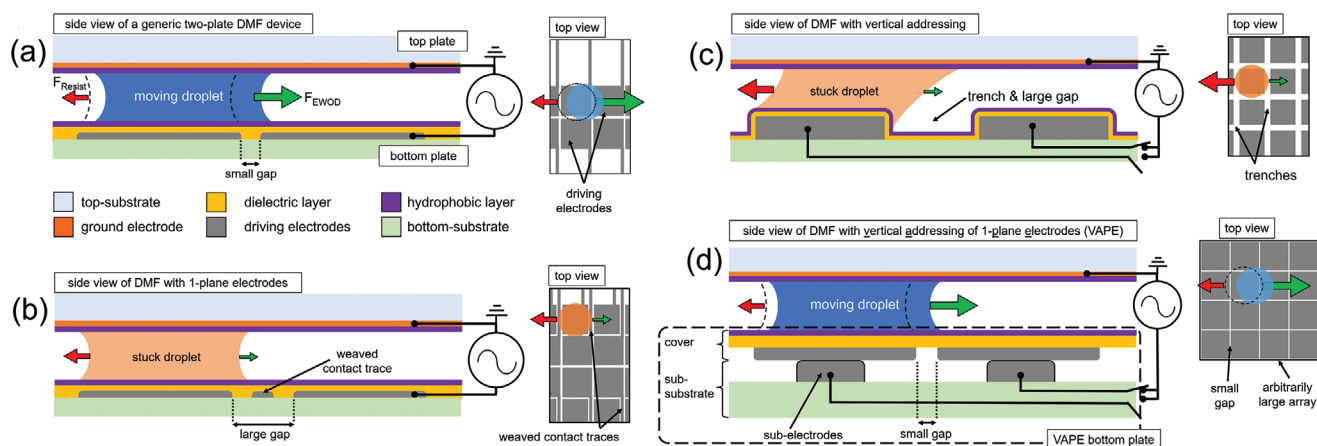


**Figure 1.** Side-view (left) and top-view (right) schematics of digital microfluidics (DMF) devices. a) Schematics of a generic two-plate DMF device, comprising a bottom substrate (green) with patterned driving electrodes (dark gray) coated with dielectric (yellow) and hydrophobic (purple) layers, and a top plate substrate (light gray) with ground electrode (orange) coated with a hydrophobic layer. When an electric potential is applied between a driving electrode and the ground electrode, an electrostatic force (“electrowetting force”  $F_{EWOD}$ , represented by the green arrow) is experienced by a droplet adjacent to the driving electrode. If  $F_{EWOD}$  exceeds the resistive force ( $F_{Resist}$ , represented by the red arrow), the droplet moves onto the driving electrode. b) Schematics of a DMF device formed by 1-plane-electrode fabrication. The requirement of “weaving” the conductive traces that connect to central electrodes increases the distance (gap) between driving electrodes, reducing  $F_{EWOD}$ —this can result in droplets becoming immobile (stuck). c) Schematics of a printed circuit board (PCB) DMF device with vertical addressing. Standard PCB-DMF devices have deep and wide trenches between adjacent electrodes, reducing  $F_{EWOD}$  and increasing  $F_{Resist}$ —this can result in droplets becoming immobile (stuck). d) Schematics of a DMF device formed by vertical addressing of 1-plane electrodes (VAPE-DMF) device. In VAPE, the DMF bottom plate is formed from two pieces—the cover, a dielectric thin-film that includes the driving electrodes, and the sub-substrate, which vertically addresses the driving electrodes on the cover and connects them to the DMF control system. VAPE-DMF devices have small gaps and no trenches between electrodes, allowing for reliable droplet movement with  $F_{EWOD} > F_{Resist}$ .

contact to be made from a “bus” layer that resides below the plane of the driving electrodes. The two categories offer complementary advantages and disadvantages, as described below.

1-plane-electrode fabrication (Figure 1b) is typified by techniques such as photolithography with a single mask layer<sup>[7]</sup>, or ink-jet printing on a single flat substrate<sup>[8]</sup>. These methods are fast and inexpensive and are widely used by academic research groups to form “proof-of-concept” devices for rapid prototyping and testing. But 1-plane-electrode devices suffer from a critical limitation; each conductive trace that connects the driving electrodes of the inner rows or columns of an array must be “weaved” around the outer driving electrodes. As shown in Figure 1b, if there are too many traces woven between the electrodes, the droplet is offset from the edge of the activated electrode, reducing  $F_{EWOD}$  to an extent that the droplet does not move. This sets a practical limit on the electrode density of devices formed using these methods to a few columns (or rows) of electrodes.

The alternative to 1-plane-electrode DMF devices is the practice of using vertical addressing fabrication techniques (Figure 1c). The main advantage of this type of device architecture is that there is no need to weave the thin conductive traces around the driving electrodes, which enables the generation of very large arrays (e.g., 100 rows x 100 columns is possible). These types of devices can be formed from printed circuit boards (PCBs) or by multilayer photolithography.

PCB techniques inherently incorporate bus layers and vertical addressing of electrode arrays. There are hundreds of vendors who will accept a digital design from a user and generate any number of physical devices (ranging from hundreds to millions) at a very inexpensive price per piece. Thus, PCBs seem (superficially) to be a perfect solution to the limitations

of the 1-plane-electrode devices described above. Unfortunately, standard PCBs have a critical disadvantage for DMF; the conductive layer (copper) is relatively thick (>30  $\mu\text{m}$ ) which results in vertical “trenches” or “ruts” (in the dimension normal to the device surface) that are several micrometers-deep between the etched electrodes. As illustrated in Figure 1c, this topography increases  $F_{Resist}$ , and in addition, it causes a large lateral gap between electrodes, which reduces  $F_{EWOD}$  (similar to the case of 1-Plane Electrode devices with many woven conductive traces). Thus, droplet motion on standard/inexpensive PCBs is known to be unreliable.<sup>[9]</sup> Note that the deep trenches and large lateral gaps found in standard PCBs can be overcome by using “specialty” vendors with more precise fabrication tools or by filling the gaps with a dielectric. But PCBs sold by these specialty vendors are much more expensive—up to hundreds of dollars per piece—making them unattractive to the average user of a DMF device, who needs an inexpensive single-use consumable.

Multilayer photolithography is an alternative to PCBs that can satisfy all the necessary technological parameters indicated above for vertical addressing devices. For example, the multinational display company, Sharp Corporation<sup>[10,11]</sup> (and others<sup>[12]</sup>), has developed methods relying on thin film transistors (TFTs) that allow the formation of large arrays of DMF electrodes. However (at the moment), Sharp is not selling their devices to outside users, and it is likely that the cost of such systems will make them unjustifiable for use as a daily (disposable) tool in a biology or chemistry laboratory. Alternatively, bio/chemistry laboratories might make their own multilayer silicon wafer/cleanroom-based vertical addressing devices (as they do with 1-plane-electrode devices), but the processes are expensive and time-consuming, and are thus not suitable for most users.

Finally, there are recent reports of using inkjet-printed ink wicked into paper to make vertical connections for general microfluidic device designs<sup>[13]</sup> and for digital microfluidics.<sup>[14]</sup> This is an intriguing strategy that will surely be explored in future work, but is likely to suffer from scalability challenges relative to PCBs and other standard manufacturing processes.

In response to these challenges, we introduce a new method for forming digital microfluidic devices that combines vertical addressing with 1-plane-electrode fabrication, or “VAPE-DMF.” This method overcomes the limitations of the techniques described above, allowing for rapid and inexpensive fabrication of arbitrarily large arrays of driving electrodes with flawless droplet movement. The key principle of VAPE-DMF is the division of the DMF bottom plate substrate (which is typically one monolithic device) into two systems: (i) the cover, which includes the DMF driving electrodes, and (ii) the sub-substrate, which includes the conductive traces used to connect DMF driving electrodes to the DMF control system (Figure 1d). In VAPE-DMF, actuated droplets touch (only) the cover; therefore, the topography of the electrodes on the sub-substrate has little impact on droplet movement.

Here, we describe the details of VAPE-DMF device fabrication and provide all of the native files needed to make them (including STL files for device interfaces, GBR files for PCB layouts and DWG files for VAPE cover layouts) as Supporting Information. We characterized the performance of VAPE-DMF devices for droplet actuation, demonstrating superior performance relative to standard vertical addressing devices. Using VAPE-DMF we also demonstrate the results of a proof-of-concept assay on a device featuring a  $20 \times 16$  array of driving electrodes, which is much denser than arrays that can be formed using standard 1-plane-electrode fabrication techniques. We propose that VAPE-DMF represents a useful new development for the growing community of users and innovators of digital microfluidics and related techniques.

## 2. Results and Discussion

### 2.1. VAPE-DMF

As described in the introduction, among users of digital microfluidics (Figure 1a), neither the existing 1-plane electrode fabrication techniques (Figure 1b) nor the vertical addressing fabrication techniques (Figure 1c) is a “perfect” match for many applications. A “perfect” (but heretofore not possible) match would form devices that combine vertical addressing from a lower bus level (with the capacity to form arbitrarily large arrays of electrodes) with the geometry, topography, and flexibility in electrode shape of 1-plane-electrode devices. Vertical addressing, 1-plane electrodes digital microfluidic devices (VAPE-DMF) do just this (Figure 1d). Specifically, VAPE-DMF distributes the functions of the bottom plate between two independent sub-systems (the cover and the sub-substrate, Figure 1d), allowing the user to take advantage of specialized manufacturing technologies and technical solutions for each system. Specifically, when choosing the sub-substrate, the fabricator can simply use standard PCBs, which are inexpensive and accessible, or any other suitable method<sup>[10–14]</sup> to form vertically addressing connections. Likewise, in forming the cover, the fabricator can

choose techniques that allow for the formation of closely spaced driving electrodes with no “trenches” between them.

Note that a key feature of the cover in VAPE-DMF is that the material is intended to be thin such that it can serve as the dielectric layer on the DMF bottom plate. The idea of using a thin, pre-formed dielectric cover for DMF is not new—it has been described previously in several different formats.<sup>[15–28]</sup> A key advantage of this format: the inexpensive dielectric cover, not the entire device, is discarded after each use, minimizing waste and expense. The novelty in VAPE-DMF is: (i) unlike the previous methods, VAPE covers constitutively include the patterned arrays of driving electrodes, and (ii) VAPE covers are designed to interface with a second component (the sub-substrate) that allows for addressing arrays of electrodes with high density (by virtue of vertical addressing).

For the work described here, we designed and built conventional PCB-DMF devices (device 1, Figure S1, Supporting Information) and compared their performance to that of two VAPE-DMF devices (devices 2 and 3, Figures S2 and S3, Supporting Information). All of the files needed to generate and use these devices, including custom vacuum manifolds (STL Files S1–S3, Supporting Information), PCB layouts (Zip Files S4–S6, Supporting Information, including GBR-format layouts), and VAPE-cover layouts (DWG Files S7–S8, Supporting Information), are provided as Supporting Information. For the former (device 1), bottom plates were formed from custom PCBs generated by an external vendor (Shenzhen JDB Technology Co., LTD), using standard materials and resolutions (i.e., electrodes were formed from  $\approx 35 \mu\text{m}$  thick copper and featured inter-electrode gaps of  $\approx 150 \mu\text{m}$ ). After receipt, PCBs were then modified with dielectric and hydrophobic layers similar to what has been described previously.<sup>[22,23,29–31]</sup> For the latter (devices 2 and 3), the sub-substrates were PCBs generated by the same external vendor (using the same materials and resolutions), featuring simple “circular” sub-electrodes, with large gaps ( $>1 \text{ mm}$ ) between them. In all of the PCBs, a solder-mask layer partially filled the gaps between electrodes, such that the trench depths (between the top of the electrode and the top of the solder mask below) were  $\approx 10 \mu\text{m}$ . Finally, the covers for devices 2 and 3 were generated from a thin ( $75 \mu\text{m}$ ) aluminum-coated polyimide film (Kapton, Dunmore Aerospace), with electrodes patterned using standard photolithography and etching. In the future, many other materials and patterning techniques (e.g., inkjet printing on flexible printing media<sup>[8,32–35]</sup>) might be used for this purpose.

A custom vacuum manifold (Figure 2) was designed and built to allow for connection of VAPE covers to VAPE sub-substrate for droplet actuation. This is a convenient arrangement, as a fresh experiment can be initiated by releasing the vacuum, removing an “old” cover, replacing it with a “new” cover, and applying the vacuum again. But in the future, many other techniques (including the use of conductive adhesive films to form vertical interconnects) might be used. Figure 2a,b illustrates the concept of a vacuum manifold and implementation of the VAPE-DMF scheme (Figure 1d) to temporarily mount the VAPE cover. Figure 2c illustrates the appearance of the VAPE-DMF device when the vacuum is engaged. In this state, the cover is pulled flat against the sub-substrate with no wrinkles, making electrical connections between the square driving electrodes

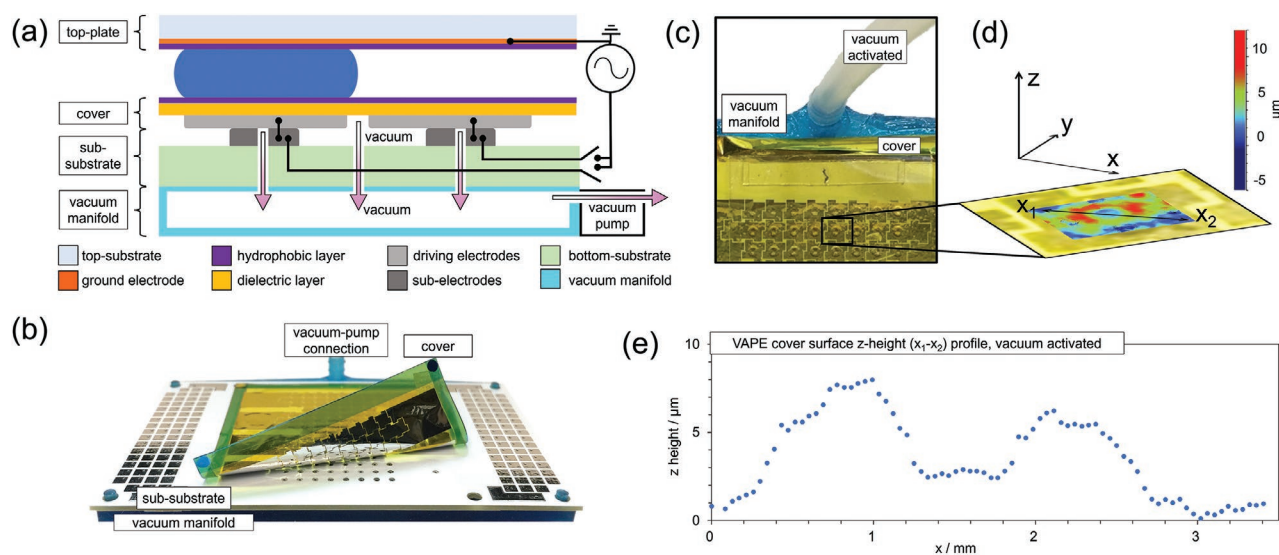


**Figure 2.** Digital microfluidics devices using vertical addressing of 1-plane electrodes (VAPE-DMF) implementation with a vacuum manifold. a) Schematic of a vacuum VAPE-DMF device (sub-substrate: green/dark-gray; cover: purple/yellow/light-gray) mounted on a vacuum manifold. b) Photograph of a representative (device 2) VAPE-DMF bottom plate. On the bottom: vacuum manifold 2 (blue) with four alignment pins (one in each corner) and a vacuum-pump connector. In the middle: the printed circuit board (PCB) sub-substrate with square contact pads and circular sub-electrodes (dark-gray), and four outer (vacuum-manifold alignment) and four inner (cover alignment) through-holes. On the top: the VAPE cover made of polyimide/aluminum (yellow/gray) with a rectangular frame of dicing tape (turquoise), and four circular optical alignment marks, one in each corner. c) Close-up photograph of an activated vacuum-pump connection (top) and a small region of VAPE-DMF “device 2” (bottom). d) Rotated close-up photo with an overlay of a 2D optical profilometry scan (with heat map height varying from low-blue to high-red) of the indicated driving electrode (on the cover) in c, with defined coordinate system and surface points  $X_1$  and  $X_2$ . e) 1D surface profile of the line extending between  $X_1$  and  $X_2$  in d, plotting height ( $z$ -axis,  $\mu\text{m}$ ) against position along the line ( $x$ -axis, mm).

(on the cover) and the circular sub-electrodes (on the sub-substrate). When assembled with a top plate for use in droplet manipulations, droplet movement was found to be facile and reliable, with no (qualitative) difference observed relative to standard 1 plane electrode devices that are commonly used in the lab. Furthermore, in the course of hundreds of experiments with VAPE-DMF devices, no sparks or arcing was observed, suggesting that tight, reliable connections are made between the electrodes on the covers and the sub-substrates.

Note that vacuum-interconnects for affixing flexible thin films to DMF electrodes have been reported previously<sup>[20]</sup>, but this is the first report that we know of in which a film bearing patterned driving electrodes (i.e., a VAPE cover) has been affixed in this manner (Figure 2b). In the present work we demonstrated the performance of VAPE-DMF with glass top-plates, but in the future less expensive alternatives (e.g., flexible PET-ITO) could bring the cost of the consumable device to the range of a few cents. Despite the above-mentioned advantages, the use of an active vacuum is not ideal for long-term use. Therefore, future iterations of VAPE-DMF, may include other adhesion methods or better sealing such that static vacuum (e.g., using a syringe) will suffice.

Another unique characteristic of the implementation of VAPE-DMF described here was the presence of topographical features arising from the unevenness of the sub-substrates. As indicated above, the PCB electrodes used here extended  $\approx 10 \mu\text{m}$  above the height of the surrounding solder-mask layer—this height difference is the source of the “trench” effect in conventional PCB devices, per Figure 1c. When assembled into a vacuum VAPE-DMF system, this resulted in the formation of “doughnut” imprints where the cover hugged the edges of the sub-electrodes,

as illustrated in Figure 2c–e. Interestingly, this topography did not appear to effect droplet movement, likely because the imprints were located at the centers of the driving electrodes, and not at the edges, where droplet movement failure is typically observed on DMF devices (per Figure 1b,c). In the future, the imprints might be minimized by using a stiffer or thicker film to form the cover or a PCB with better surface quality, but even with the imprints, the performance of VAPE-DMF was found to be far superior to that of traditional PCB DMF, as described below.

## 2.2. VAPE-DMF Performance

A continuous movement test was developed to quantitatively evaluate the reliability of droplet movement on conventional PCB-DMF devices and VAPE-DMF devices. The test, termed a “translation-step experiment” illustrated in Figure 3a; as shown, a droplet is continuously driven through a series of six steps (steps I–VI) to complete a full revolution. In typical tests, 50 revolutions (300 steps) were carried out, meanwhile the average droplet velocity was logged continuously via capacitive sensing.<sup>[36]</sup> As shown in Figure 3b, in some cases, a given droplet became stuck/immobile, leading to a recorded velocity of “zero.” The pre-programmed circular path ensured that a single step failure would not cause the entire revolution to fail, as an immobile droplet in one step could resume the movement at a later step in which a different electrode adjacent to the droplet was actuated. To ensure fair comparison, devices with identical layouts (device 1/Figure S1, Supporting Information and device 2/Figure S2, Supporting Information) were used.

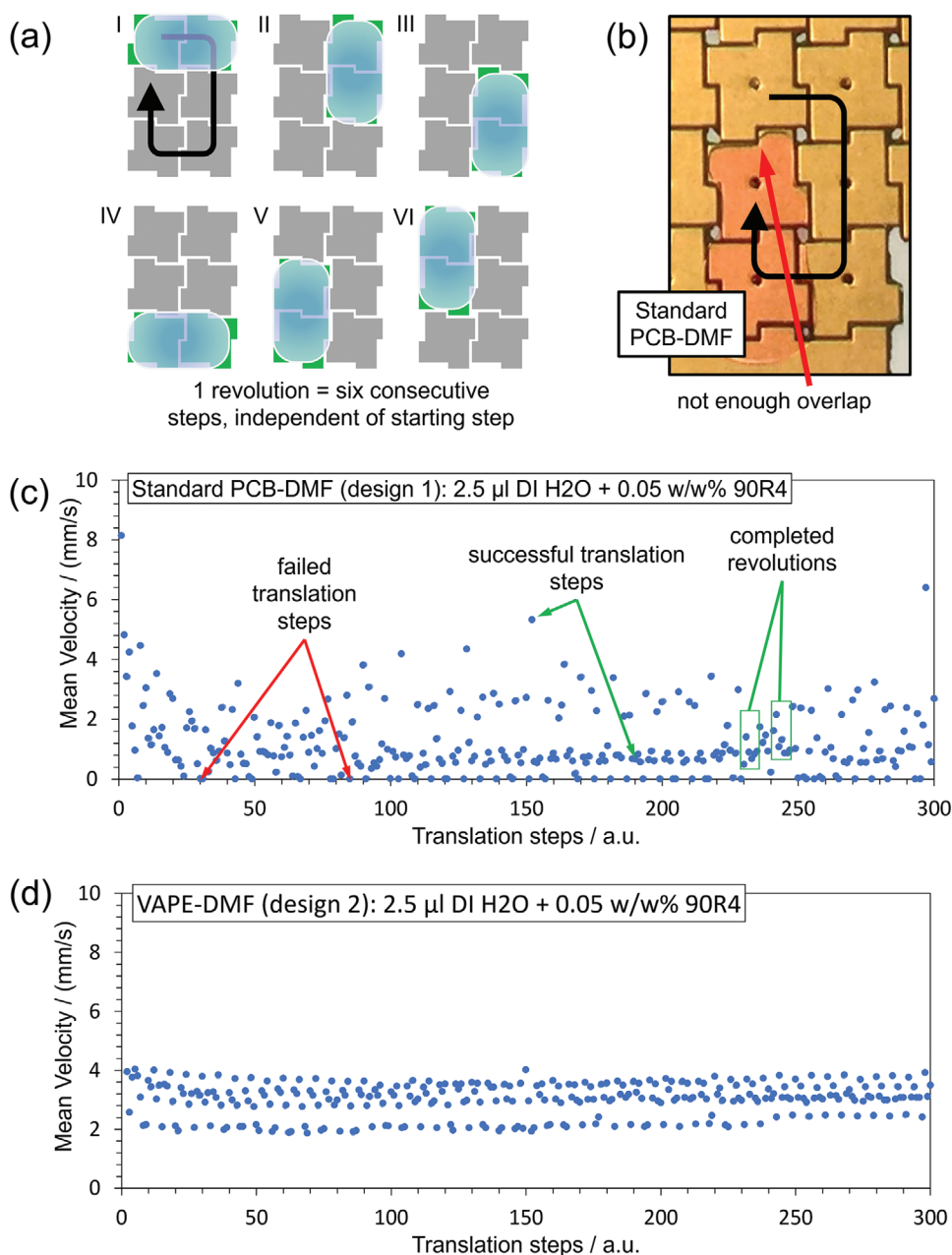


**Figure 3.** Translation-step experiments for printed circuit board (PCB) digital microfluidics (DMF) and DMF devices using vertical addressing of 1-plane electrodes (VAPE-DMF). a) Cartoon of test in which a droplet (blue) revolves around a  $2 \times 3$  array of driving electrodes (gray). Two adjacent electrodes are activated (green) during each translation step. b) Example photograph of a translation-step failure (with an immobile droplet) on a standard PCB-DMF device. A red arrow indicates the inability of the droplet to overlap the adjacent electrode, required to facilitate droplet movement upon actuation. c,d) Translation-step droplet velocity plots (blue markers) generated from a standard PCB-DMF device (device 1) (c) and a VAPE-DMF device (device 2) (d). Examples of failed translation steps (in which the droplet remained immobile) and successful translation steps are highlighted with red and green arrows, respectively. Examples of completed revolutions (with six consecutive successful steps) are highlighted in green boxes. Experiment parameters: 2.5  $\mu$ L DI H<sub>2</sub>O + 0.05% w/w 90R4, inter-plate spacer height  $\approx$ 200  $\mu$ m, actuation AC voltage 130 V at 10 kHz. A total of 300 translation steps correspond to 50 revolutions.

Figure 3c demonstrates the stepwise (300 translation steps) mean droplet velocity measurements using the standard PCB-DMF chip (device 1). Examples of failed translation steps, successful translation steps, and successful revolutions are marked with red arrows, green arrows, and green boxes, respectively. As shown, the standard PCB-DMF chip (device 1) successfully

completed only 253 out of 300 steps. In contrast, the VAPE-DMF chip (device 2) successfully completed 300 of 300 steps (Figure 3d).

As indicated, droplet movement failure is far less likely in VAPE-DMF devices than in conventional PCB-DMF devices. In fact, in the course of hundreds of experiments with VAPE-DMF devices, we have not observed any droplet movement failures.

Beyond failure, the droplet velocity is also far more consistent in VAPE-DMF devices. For example, the average velocity for 300 movement steps in VAPE-DMF was  $3.01 \text{ mm s}^{-1}$  with a relative standard deviation (RSD) of 19.0%. Interestingly, this noise level was small enough to resolve velocity trends that correlate with repeated steps during each revolution. Specifically, VAPE-DMF steps (I–VI) exhibited the following average droplet velocities  $\pm$  RSDs: (I)  $2.96 \text{ mm s}^{-1} \pm 3.6\%$ , (II)  $2.62 \text{ mm s}^{-1} \pm 20.5\%$ , (III)  $2.18 \text{ mm s}^{-1} \pm 8.6\%$ , (IV)  $3.57 \text{ mm s}^{-1} \pm 74\%$ , (V)  $3.15 \text{ mm s}^{-1} \pm 74\%$ , and (VI)  $3.59 \text{ mm s}^{-1} \pm 4.4\%$ . The numbers above suggest that, other than step (II), the observed stepwise variances in droplet velocity were quite small ( $<9\%$  RSD). These minute variations might alternatively be attributed to poorly regulated variations in the applied actuation voltages or unwanted lags between steps. In contrast, the average droplet velocity during the 253 successful movement steps performed with the conventional PCB-DMF (ignoring the 47 steps with zero velocity) was  $1.44 \text{ mm s}^{-1}$  with a RSD of 78.5%; this noiseband prevents us from identifying any velocity trends related to the step number. In sum, it is clear that

droplet movement in VAPE-DMF is far more reliable and repeatable than in standard PCB-DMF, making VAPE-DMF attractive for applications, as described below.

### 2.3. VAPE-DMF Application

To evaluate the capacity of the new method for multiplexing, we tested VAPE-DMF devices with an application requiring 24 concurrent mixing operations. A device with an array of 336 electrodes (featuring a continuous  $16 \times 20$  array of electrodes) was designed and fabricated (“device 3”, Figure S3, Supporting Information). The packing of adjacent electrodes in such device greatly exceeds the limits of any conventional 1-plane electrode fabrication method. An assay that featured prominently in the early history of DMF (demonstrated by Srinivasan et al. in 2004<sup>[1,4]</sup>), the Trinder reaction for glucose determination (Figure 4a), was used as a “test case” for the new VAPE-DMF system. The previous reports<sup>[1,4]</sup> featured a 1-plane device layout

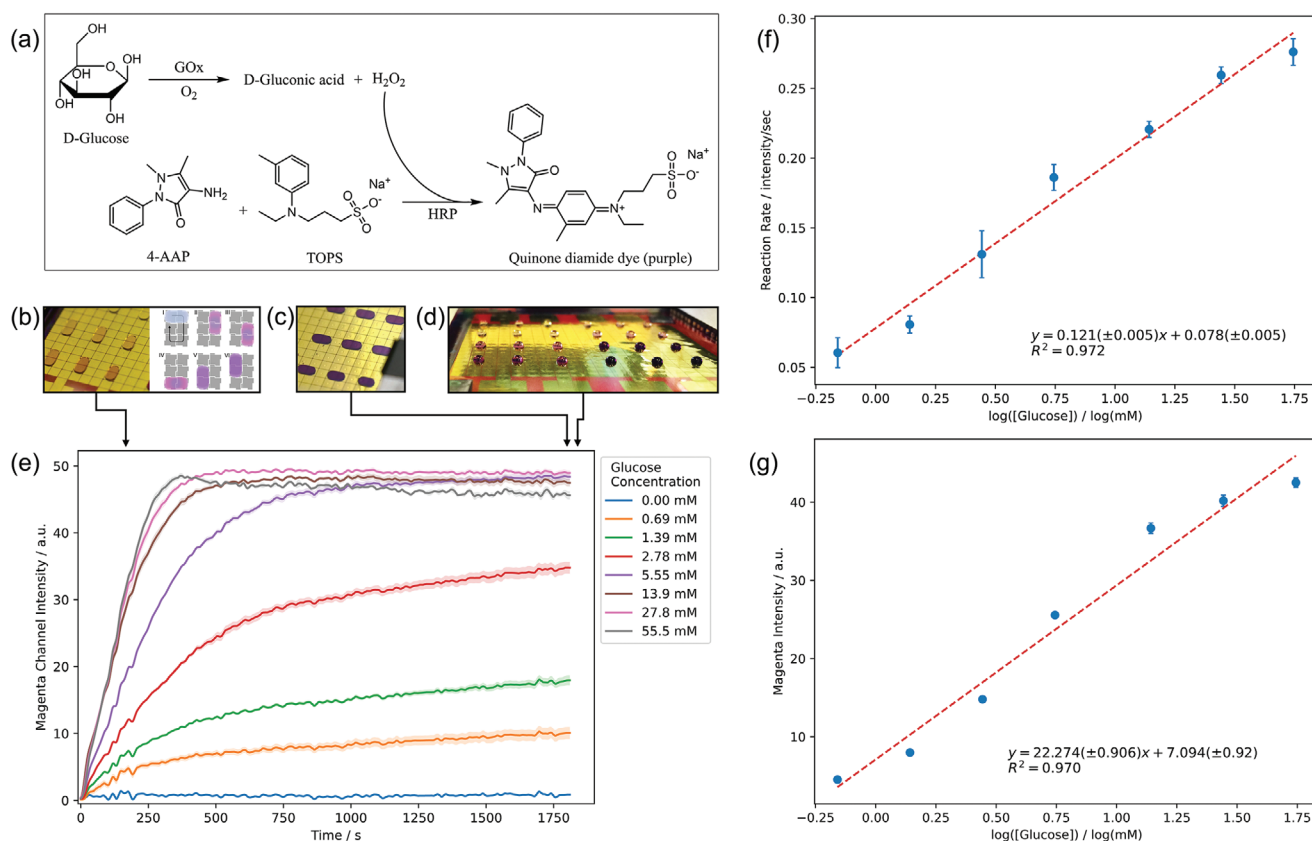


**Figure 4.** Digital microfluidics (DMF) devices using vertical addressing of 1-plane electrodes (VAPE-DMF) parallel-scale reactions. a) Reaction scheme of the Trinder reaction. D-glucose is converted to D-gluconic acid and hydrogen peroxide, catalyzed by glucose oxidase (GOx). Hydrogen peroxide reacts with 4-aminoantipyrine (4-AAP) and 3-(N-ethyl-3-methylanilino)propane-1-sulfonic acid sodium salt (TOPS) to produce a colored quinone diamide product, catalyzed by horseradish peroxidase (HRP). b) Representative photograph (left) of a portion of VAPE-DMF device 3, showing a sub-set of glucose reaction-droplets after 2 min, and cartoon (right) illustrating the six-step active mixing procedure that was applied to each reaction. c) Representative photograph of a portion of VAPE-DMF device 3, showing a sub-set of glucose reaction-droplets after 29 min. d) Photograph of an entire VAPE-DMF device 3 with top plate removed, showing 24 glucose reaction-droplets after 30 min. e) Graph of the pixel intensity of the magenta channel versus time for each glucose concentration. Shaded regions represent the  $\pm 1$  std. dev. for  $n = 3$  replicates per concentration. f) Plot of reaction rate determined from the first 25 s of the reaction as a function of the logarithm of glucose concentration. g) Plot of blank-subtracted pixel intensity measured 256 s after the start of the reaction as a function of the logarithm of glucose concentration. Measured data (f,g) are shown as blue markers (error bars represent  $\pm 1$  std. dev. from  $n = 3$  replicates), and linear regressions are shown as red dashed lines, with equations and  $R^2$  indicated at the bottom of each plot.

of electrodes arranged in a single series, which was sufficient to run two reactions at a time. In contrast, the new densely packed 336-electrode VAPE-DMF device had more than enough electrodes to run 24 reactions in parallel. While the majority of the DMF literature describes single-droplet detectors (e.g., Srinivasan et al. used an LED/photodiode pair<sup>[1,4]</sup> sufficient to test one droplet at a time), to take advantage of the parallel nature of VAPE-DMF, a new multiplexed detection scheme was used here, in which an inexpensive webcam was used to record videos. Each frame was then converted to CMYK and decoded to determine the relative level of product that accumulated over time for all of the droplets in parallel.

In practice, each VAPE-DMF Trinder-reaction experiment required the capacity to handle 48 droplets—21 glucose standards, 3 blanks, and 24 reactant mixes. As shown in Figure 4b, each sample (standard or blank)—reaction mix pair was merged and then mixed in a six-step pre-programmed path—identical to the translation-step method illustrated in Figure 3a. As time progressed (Figure 4c,d and Movie File S9, Supporting Information), the reaction product was quantified as an increase in the pixel intensity of the Magenta channel of each droplet (noting that the quinone diamide product has  $\lambda_{\max} = 550 \text{ nm}$ <sup>[37,38]</sup>). Pre-defined regions of interest (ROIs) allowed for near real-time monitoring of the reaction, indicating that this type of image processing can be used in line with the recorded video feed. Data were evaluated as a function of reaction rate determined during the first 25 s of the reaction (Figure 4e) or in an endpoint detection scheme after an empirically determined reaction time of  $t = 256 \text{ s}$  (Figure 4f), with  $R^2$  values of 0.972 and 0.970, respectively. The limits of detection (LODs) for the two techniques were  $0.553 \times 10^{-3} \text{ M}$  ( $10 \text{ mg dL}^{-1}$ ) and  $1.038 \times 10^{-3} \text{ M}$  ( $18.7 \text{ mg dL}^{-1}$ ) D-glucose, respectively, which is comparable to what has been reported previously for microfluidic spectrophotometry.<sup>[4]</sup>

### 3. Conclusion

We introduce a new method for forming digital microfluidic devices, VAPE-DMF, which divides the functions of the DMF bottom-plate into two independent systems: (1) the cover, a dielectric thin-film that includes the actuation electrodes, and (2) the sub-substrate, which vertically addresses the actuation electrodes and connects them to the DMF control system. VAPE-DMF enables fast, cost-, environment-, material-, and time-efficient fabrication and use of DMF devices. We demonstrated the potential of this technique by exercising parallel control of 48 droplets to perform 24 individual Trinder reactions for glucose sensing simultaneously. We propose that the new technique will be useful for users and innovators alike who are interested in improving the throughput of their DMF assays.

### 4. Experimental Section

**Reagents:** Unless otherwise specified, reagents were purchased from SigmaAldrich, and electronic components were purchased from Digi-Key. Deionized water (DI H<sub>2</sub>O) with a resistivity of >18 megohm cm was used to prepare all aqueous solutions. All solutions were supplemented with 0.05% w/w ethylenediaminetetrakis(ethoxylate-block-propoxylate) tetrol (Tetronic 90R4, BASF Corp.).

**Custom Vacuum Manifolds:** Three custom vacuum manifolds were designed and built for the work described here. Manifold 1 was designed with AutoDesk Inventor (STL File S1, Supporting Information) to interface with a spin-coater (Laurell Technologies Corporation) to allow for spin-coating of flexible, rectangular films. Manifold 2 (STL File S2, Supporting Information) was designed with AutoDesk AutoCAD to mount device 2 (details below) for VAPE-DMF operations and features an array of 64 through-holes (1 mm diameter) connected to a chamber that terminates in a fitting to interface with 3.5 mm i.d. tubing to connect to a vacuum pump. The array is surrounded by four vertical alignment pins (2 mm diameter, spaced 71.2 and 45.7 mm from each other). Manifold 3 was designed with AutoDesk Inventor (STL File S3, Supporting Information) to mount device 3 (details below) for VAPE-DMF operations and features an array of 336 through-holes (1 mm diameter, spaced to interface with electrodes on device 3) connected to a chamber that terminates in a fitting to interface with 3.5 mm i.d. tubing to connect to a vacuum pump. The array is surrounded by four outer (1.8 mm diameter, spaced 71 mm from each other) and four inner (1.8 mm diameter, spaced 35 and 65 mm from each other) vertical alignment pins. Each vacuum manifold was 3D printed in FLTOTL05 resin using a Form 2 3D printer (Formlabs). Post-printing, the manifolds were washed two times in isopropanol for 10 min to remove any un-crosslinked resin, dried with pressured air to clear the inner channels, and then cured under UV light for 2 h at 80 °C.

**Printed Circuit Boards:** Three PCB device designs were formed in the open-source software suite KiCAD (www.kicad-pcb.org): device 1 (2" × 3" conventional PCB-DMF bottom plate), device 2 (2" × 3" VAPE sub-substrate), and device 3 (3" × 3" VAPE sub-substrate). Device 1 (Figure S1, Supporting Information) featured 120 driving electrodes, including 104 roughly square driving electrodes (2.5 × 2.5 mm), arranged in 15 rows with an average of 6.9 columns (that is, rows 1–7 had 8, 6, 8, 6, 8, 6, and 8 electrodes, row 8 had four electrodes, and rows 9–15 were identical to rows 1–7). The driving electrode array was surrounded with eight roughly rectangular dispensing electrodes (2.5 × 5 mm), and eight roughly rectangular reservoir electrodes (5 × 7.5 mm). The driving electrodes featured an irregular interdigitation pattern similar to what is reported by Dixon et al.<sup>[2]</sup>, but scaled up such that the driving electrodes have a pitch of 2.54 mm and inter-electrode gaps of 150 μm. Device 2 (Figure S2, Supporting Information) featured 120 circular 1 mm dia. sub-electrodes with pitch designed to align with the device 2 VAPE cover (see details below). The device also included four outer-alignment through-holes (2.2 mm diameter) spaced to mate with the pins in vacuum manifold 2, and four inner-alignment holes (2.2 mm diameter) spaced to fit the visual alignment marks of a device 2 VAPE cover (see below). Device 3 (Figure S3, Supporting Information) featured 336 circular 1 mm dia. sub-electrodes with pitch designed to align with the device 3 VAPE cover (see below). The device also included four outer alignment through-holes (2.2 mm diameter) spaced to mate with the pins in vacuum manifold 2, and four inner alignment through-holes (2.2 mm diameter) spaced to fit the alignment holes of a device 3 VAPE cover (Figure S3, Supporting Information). In the three PCBs, each driving electrode or sub-electrode on the top layer was connected (by vertical addressing through 0.3 mm diameter through-holes to a bus layer below the top layer) to a contact pad located on either the left or right edge of the device. Contact pads were laid out in two arrays (to the left and right of the driving electrode arrays) designed to mate with the DropBot interface design, described elsewhere.<sup>[36]</sup> For devices 1–2, each electrode or sub-electrode was connected to a unique contact pad. For device 3, the 320 sub-electrodes in the center of the array (laid out in a 16 × 20 array of rows and columns) were divided into four analogous 8 × 10 sub-arrays, and each electrode in each of the sub-arrays was connected in parallel to the same contact pad. The remaining 16 sub-electrodes of device 3 were connected to unique contact pads to address eight reservoir electrodes and eight dispensing electrodes independently.

The PCBs were fabricated by PCBway (Shenzhen JDB Technology Co., LTD). Device 1 (ZIP File S4, Supporting Information) specifications were: 2 layers, thickness 1 mm, no silkscreen, surface finish HASL with lead, vias not covered, material FR-4 TG130, solder mask matt black

between copper, finish copper 1 oz ( $\approx 35 \mu\text{m}$  thick). Device 2 (ZIP File S5, Supporting Information) specifications were: 2 layers, thickness 1 mm, no silkscreen, surface finish immersion gold, vias not covered, material FR-4 TG170, solder mask white between copper, finish copper 1 oz ( $\approx 35 \mu\text{m}$  thick). Device 3 (ZIP File S6, Supporting Information) specifications were: 6 layers, thickness 1.6 mm, no silkscreen, surface finish immersion gold, vias not covered, material FR-4 TG150, solder mask red between copper, finish copper 1 oz ( $\approx 35 \mu\text{m}$  thick). The PCBs used for VAPE-DMF sub-substrates (devices 2–3) were used as received; PCBs used for conventional DMF bottom plates (device 1) were coated with a dielectric layer of  $8 \mu\text{m}$  thick Parylene-C using chemical vapor deposition, and a hydrophobic layer [0.5 wt% FluoroPolymer PFC 1104V (Cytonix) in PFC 110 Fluoro Solvent (Cytonix), spin-coated (2000 rpm, 60 s), and dried at room temperature].

**VAPE-DMF Bottom-Plate Covers:** VAPE-DMF bottom-plate covers were fabricated at the University of Toronto Nanofabrication Centre (TNFC) from  $7.5 \mu\text{m}$  thick polyimide film bearing vapor-deposited aluminum on one side with sheet resistance  $0.67 \Omega \text{ sq}^{-1}$  (DE300 VDA/30GA Kapton HN, Dunmore Aerospace). The film was cut into  $\approx 70 \times 100 \text{ mm}$  pieces, and the aluminum side of each piece was gently cleaned with isopropanol. The pieces were then affixed (aluminum side up) with dicing-tape (Semiconductor Equipment Corporation, CA) onto  $75 \times 75 \text{ mm}$  glass slides (wrapping excess film around each slide) to provide mechanical support during coating and washing. Photoresist S1811 (Microchem) was spin-coated onto the unprotected aluminum layer of each piece (2000 rpm for 30 s), and then was soft-baked on a hotplate at  $95 \text{ }^\circ\text{C}$  for 60 s. Each piece was exposed through a photomask [printed using a uPG 501 mask writer (Heidelberg Instruments Mikrotechnik GmbH, Germany) in the Center for Microfluidic Systems at the University of Toronto] for 6 s in a Suss MicroTec MA6 Mask Aligner, followed by developing in Microposit MF-312 (diluted 1:1) for 45 s, rinsing in DI  $\text{H}_2\text{O}$  and drying under nitrogen. Each piece was then immersed in Aluminum Etchant Type D (SigmaAldrich) until the electrode pattern was observed to develop. The pieces were then rinsed in DI  $\text{H}_2\text{O}$ , the photoresist was stripped using AZ 300T Stripper, and if necessary, the pieces were additionally de-scummed by brief exposure to acetone and isopropanol to remove persistent photoresist residues. Subsequently, the pieces were rinsed in DI  $\text{H}_2\text{O}$ , and dried using nitrogen. The dicing tape was removed, and each cover was detached from the glass slide.

When complete, each device 2 VAPE cover (Figure S2, Supporting Information) featured 104 roughly square driving electrodes ( $2.5 \times 2.5 \text{ mm}$ ), eight roughly rectangular dispensing electrodes ( $2.5 \times 5.0 \text{ mm}$ ), and eight roughly rectangular reservoir electrodes ( $10 \times 7.5 \text{ mm}$ ), with interdigitation and layout similar to that of device 1 bottom plates, and inter-electrode gaps of  $100 \mu\text{m}$  (DWG File S7, Supporting Information). When complete, each device 3 VAPE cover (Figure S3, Supporting Information) featured 320 square driving electrodes ( $2.5 \times 2.5 \text{ mm}$ ) laid out in a  $16 \times 20$  array of rows and columns, eight rectangular dispensing electrodes ( $2.5 \times 5 \text{ mm}$ ), and eight roughly rectangular reservoir electrodes ( $6.0 \times 4.5 \text{ mm}$ ). Electrode interfaces on the cover featured modest interdigitation (sine waves with wavelength  $\approx 200 \mu\text{m}$  and p-p amplitude  $\approx 100 \mu\text{m}$ ) and inter-electrode gaps of  $30 \mu\text{m}$  (DWG File S8, Supporting Information). As illustrated in Figures S2 and S3 (Supporting Information), each cover also includes circular alignment marks distributed around the electrode arrays.

After formation of the electrode arrays, each cover was positioned (electrodes down) on a clean  $200 \times 200 \text{ mm}$  acrylic tile with a small amount of IPA between tile and cover. Four strips of dicing tape ( $\approx 10 \times 75 \text{ mm}$  ea.) were applied to the edges of the cover to form a rectangular frame (with an “opening” of  $\approx 44 \times 44 \text{ mm}$  for device 2 and  $\approx 64 \times 44 \text{ mm}$  for device 3), with the driving electrode array centered in the middle of the opening. A rectangular section of cover and dicing tape was cut with a scalpel and removed from acrylic tile ( $\approx 50 \times 50 \text{ mm}$  for device 2 or  $70 \text{ mm} \times 50 \text{ mm}$  for device 3). A 2 mm biopsy punch (Integra Miltex) was used to perforate the cover at the alignment marks. Finally, each cover was placed (electrode-side down) on custom vacuum manifold 1 and spin-coated coated with 0.5 wt% FluoroPolymer PFC 1104V (Cytonix) in PFC 110 Fluoro Solvent (Cytonix) at 2000 rpm for 60 s, followed by drying at room temperature.

**Top Plates:** ITO coated glass slides  $75 \times 25 \times 1 \text{ mm}$  and  $75 \times 50 \times 1 \text{ mm}$  (Delta Technologies, Inc.) were used to form DMF top plates.

Briefly, slides were cleaned by rinsing with acetone, isopropanol, and DI  $\text{H}_2\text{O}$ , and dried with compressed nitrogen gas. Each piece was spin-coated with 0.5 wt% Teflon AF 1600 (DuPont) in Fluorinert FC-40 at 2000 rpm for 60 s, and baked on a hotplate for 10 min at  $170 \text{ }^\circ\text{C}$ .

**DMF Device Assembly and Operation:** Device 1 (conventional PCB-DMF) bottom plates were joined to top plates by spacers formed from two layers of Scotch Brand double sided tape (3M) ( $\approx 200 \mu\text{m}$  thick total). Device 2 and device 3 VAPE sub-substrates and covers were assembled into functioning bottom plates by sliding them onto the pins of the custom vacuum manifolds 2 and 3, respectively. The vacuum manifolds were then connected via PTFE tubing (4 mm o.d. 3.5 mm i.d.) to a vacuum pump (DOA-P704-AA, Gast Manufacturing Inc.), and the vacuum pump was kept activated for the duration of each experiment. The device bottom plates were then joined to top plates as described above. Note that the particular combination of bottom and top plates reported here (coated with Fluoropel and Teflon-AF, respectively) was selected by accident, and in limited experiments, other combinations (all Fluoropel, all Teflon-AF, and others) were found to behave similarly.

All devices were interfaced through pogo-pin connectors to a Drop-Bot digital microfluidic control system running MicroDrop software, which is described in detail elsewhere.<sup>[36]</sup> Droplets were actuated by applying sine waves of up to  $155 \text{ V}_{\text{RMS}}$  at 10 kHz between the top-plate electrode and successive electrodes on the bottom plate, in pre-programmed sequences. In all cases force–velocity curves were collected, to guide selection of driving potentials that resulted in high, but sub-saturation driving forces.<sup>[6]</sup>

**Device Surface Characterization:** Device 3 VAPE sub-substrates and covers were assembled into functioning bottom plates and placed on vacuum manifold 3. The manifold was then connected (PTFE tubing, 4 mm o.d. 3.2 mm i.d.) to a syringe (30 mL, VWR), which was used to create and hold a vacuum during the measurement ( $\approx 30 \text{ s}$ ). The VAPE device was characterized with an optical profilometer (Contour GT-K, Bruker Corporation), using a 10x objective and a 0.55x tube lens to scan an area of  $2.3 \times 3.0 \text{ mm}$ , centered over the sub-electrode’s imprint on the VAPE cover. A color-coded surface height-profile image was compiled from the scanning data and a one-dimensional height-profile was extracted using the Vision64 operating software (Bruker Corporation).

**Translation-Step Experiments:** Translation-step experiments were performed using PCB-DMF device 1 and VAPE-DMF device 2 to manipulate  $2.5 \mu\text{L}$  droplets (“double-unit droplets” with volume sufficient to cover two driving electrodes) of DI  $\text{H}_2\text{O}$  supplemented with 0.05% w/w 90R4. Briefly, a MicroDrop<sup>[36]</sup> step sequence was written to translate a droplet in clockwise revolutions around a  $2 \times 3$  array of six driving electrodes. Each revolution comprised six translation steps (I–VI), and in each translation step, 130 V at 10 kHz was applied to two destination electrodes (step I:  $1^{\text{st}} + 2^{\text{nd}}$  driving electrode activated; step II:  $2^{\text{nd}} + 3^{\text{rd}}$  activated, ..., step VI =  $6^{\text{th}} + 1^{\text{st}}$  activated) for 3 s. The droplet position was monitored by capacitance measurements collected at 200 Hz. Each experiment proceeded until 50 revolutions (300 steps) had been completed, and the average droplet velocity of each step was recorded using MicroDrop.<sup>[36]</sup>

**Modified Trinder Reaction:** The Trinder reaction for glucose detection was implemented on VAPE-DMF device 3 using a modified version of a procedure described elsewhere.<sup>[1,4]</sup> Briefly, a master-mix solution consisted of  $12.5 \text{ IU mL}^{-1}$  glucose oxidase (GOx),  $2.5 \text{ IU mL}^{-1}$  horseradish peroxidase (HRP),  $3 \times 10^{-3} \text{ M}$  4-aminoantipyrene (4-AAP), and  $5 \times 10^{-3} \text{ M}$  3-(N-ethyl-3-methylanilino) propanesulfonic acid sodium salt (TOPS) was prepared in diluent (DI  $\text{H}_2\text{O}$  supplemented with 0.05% w/w 90R4). Standard solutions of glucose at seven different concentrations ( $0.694 \times 10^{-3}$ ,  $1.39 \times 10^{-3}$ ,  $2.78 \times 10^{-3}$ ,  $5.55 \times 10^{-3}$ ,  $13.9 \times 10^{-3}$ ,  $27.8 \times 10^{-3}$ ,  $55.5 \times 10^{-3} \text{ M}$ ) in diluent were prepared by serial dilution.

Twenty-one  $2.0 \mu\text{L}$  droplets of glucose standards (three at each concentration), three  $2.0 \mu\text{L}$  droplets of diluent (serving as a blank), and 24  $2.0 \mu\text{L}$  droplets of master-mix solution were pipetted onto an open VAPE-DMF device (mounted on the manifold with vacuum applied but without a top plate), forming 24 pairs of droplets. Each pair was separated from other pairs by at least two electrodes in either direction. A top plate was affixed, and a custom protocol was initiated in which each droplet pair merged to form a colorless  $4.0 \mu\text{L}$  reaction-droplet.



The 24 reaction-droplets were mixed for 30 min in revolutions around six electrodes following the translation-step experiment procedure. The web camera (Logitech HD Pro Webcam C920) in the DropBot (positioned 30° relative to the plane perpendicular to the DMF device) was used to capture a video for 1750 s at 30 frames s<sup>-1</sup>.

Videos were processed using a custom eight-step script written in Python 3. (1) Each video frame was loaded and treated as an RGB image (1920 × 1080 pixels). The frame count and frame rate were used to infer a timestamp for each image. (2) Each image was corrected for perspective as described previously.<sup>[39]</sup> Briefly, four coordinates in the source image were defined and paired with four predefined reference coordinates. The coordinate pairs were used to calculate a 3 × 3 matrix and then the same matrix was used to transform the source image into the perspective-corrected image. (3) The device design was used to define 24 groups of six ROIs on each image, where each ROI represented a single electrode, and each group corresponded to the mixing path of a reaction-droplet. (4) Each group of six ROIs (corresponding to a given droplet at a given timestamp) was further processed by extracting six square sub-images from the center of each ROI (each containing half the area of its parent ROI). (5) The average pixel intensity of the R, G, and B channels from each of the six sub-images was extracted and each R, G, B trio was converted to CMYK by a standard equation.<sup>[40]</sup> The maximum value in the Magenta (M) channel among the six sub-images in the group was recorded as the signal *S* at that time point. (6) An array of signal *S* as a function of time was assembled for each of the 24 reactions as a function of time, and each array was smoothed with a low-pass Butterworth filter ( $f_{\text{cutoff}} = 0.04$  Hz). The three arrays corresponding to each glucose concentration and the three arrays corresponding to the blank were averaged together, yielding eight arrays of *S* as a function of time. (7) The average signal of the blank was subtracted from the seven average signals of the glucose standards at all time points, yielding seven arrays of blank-subtracted signal *S*<sub>bs</sub> as a function of time. (8) Data were plotted as reaction rate or signal as a function of log [glucose concentration]. For the former, the data were evaluated by fitting a line to *S* in a rolling window of 3.33 s (100 data-points) across the entire dataset and recording the maximum slope. (In practice, the maximum slope was always found to be at the first 25 s of the reaction.) For the latter, the data were *S*<sub>bs</sub> for each concentration at *t* = 256 s. Data evaluated both ways were fitted by linear regression, and the LODs were determined as the concentrations corresponding to the signal that was equivalent (from the linear regression) to the average blank signal plus three times the standard deviation of the blank signal.

## Supporting Information

Supporting Information is available from the Wiley Online Library or from the author.

## Acknowledgements

The authors thank Drs. Ian Swyer, Michael Dryden, and Christopher Dixon (Univ. Toronto) for fruitful discussions.

## Conflict of Interest

S.v.d.E., A.A.S., and A.R.W. are co-inventors on a patent application that describes some of the methods reported here.

## Author Contributions

S.v.d.E. and A.R.W. developed the VAPE idea and S.v.d.E. developed the methods to manufacture and operate the devices and manufactured them. S.v.d.E. and A.A.S. designed and manufactured the vacuum manifolds, performed the Trinder reaction experiments and analyzed the data. S.v.d.E., A.A.S., and A.R.W. wrote the manuscript.

## Data Availability Statement

The data that support the findings of this study are available from the corresponding author upon reasonable request.

## Keywords

digital microfluidics, electrowetting, multiplexed analysis, thin film dielectric, Trinder reaction

Received: September 22, 2021

Revised: November 23, 2021

Published online: December 16, 2021

- [1] V. Srinivasan, V. K. Pamula, R. B. Fair, *Lab Chip* **2004**, *4*, 310.
- [2] C. Dixon, J. Lamanna, A. R. Wheeler, *Lab Chip* **2020**, *20*, 1845.
- [3] A. H. C. Ng, R. Fobel, C. Fobel, J. Lamanna, D. G. Rackus, A. Summers, C. Dixon, M. D. M. Dryden, C. Lam, M. Ho, N. S. Mufti, V. Lee, M. A. M. Asri, E. A. Sykes, M. D. Chamberlain, R. Joseph, M. Ope, H. M. Scobie, A. Knipes, P. A. Rota, N. Marano, P. M. Chege, M. Njuguna, R. Nzunza, N. Kisangau, J. Kiogora, M. Karuingi, J. W. Burton, P. Borus, E. Lam, A. R. Wheeler, *Sci. Transl. Med.* **2018**, *10*, eaar6076.
- [4] V. Srinivasan, V. K. Pamula, R. B. Fair, *Anal. Chim. Acta* **2004**, *507*, 145.
- [5] M. G. Pollack, R. B. Fair, A. D. Shenderov, *Appl. Phys. Lett.* **2000**, *77*, 1725.
- [6] I. Swyer, R. Fobel, A. R. Wheeler, *Langmuir* **2019**, *35*, 5342.
- [7] K. Choi, A. H. C. Ng, R. Fobel, A. R. Wheeler, *Annu. Rev. Anal. Chem.* **2012**, *5*, 413.
- [8] C. Dixon, A. H. C. Ng, R. Fobel, M. B. Miltenburg, A. R. Wheeler, *Lab Chip* **2016**, *16*, 4560.
- [9] M. Abdelgawad, A. R. Wheeler, *Adv. Mater.* **2007**, *19*, 133.
- [10] B. Hadwen, G. R. Broder, D. Morganti, A. Jacobs, C. Brown, J. R. Hector, Y. Kubota, H. Morgan, *Lab Chip* **2012**, *12*, 3305.
- [11] S. Anderson, B. Hadwen, C. Brown, *Lab Chip* **2021**, *21*, 962.
- [12] Y. Xing, Y. Liu, R. Chen, Y. Li, C. Zhang, Y. Jiang, Y. Lu, B. Lin, P. Chen, R. Tian, X. Liu, X. Cheng, *Lab Chip* **2021**, *21*, 1886.
- [13] M. M. Hamed, A. Ainla, F. Güder, D. C. Christodouleas, M. T. Fernández-Abedul, G. M. Whitesides, *Adv. Mater.* **2016**, *28*, 5054.
- [14] A. T. Jafry, H. Lee, A. P. Tenggara, H. Lim, Y. Moon, S.-H. Kim, Y. Lee, S.-M. Kim, S. Park, D. Byun, J. Lee, *Sens. Actuators, B* **2019**, *282*, 831.
- [15] M. Abdelgawad, A. R. Wheeler, *Microfluid. Nanofluid.* **2008**, *4*, 349.
- [16] H. Yang, V. N. Luk, M. Abdelgawad, I. Barbulovic-Nad, A. R. Wheeler, *Anal. Chem.* **2009**, *81*, 1061.
- [17] A. R. Wheeler, I. Barbulovic-Nad, H. Yang, M. Abdelgawad, *US8187864B2*, **2010**.
- [18] Kai-Cheng Chuang, Shih-Kang Fan, in *19th IEEE Int. Conf. on Micro Electro Mechanical Systems*, IEEE, Piscataway, NJ **2006**, pp. 538–541.
- [19] M. Alistar, U. Gaudenz, *Bioengineering* **2017**, *4*, 45.
- [20] M. N. Feiglin, *WO/2014/187488A1*, **2014**.
- [21] J. A. Soto-Moreno, I. P. Hong, J. G. Beltran-Vera, J. M. Decarli, J. A. Quintero, R. Wilhelmy-Preciado, M. J. Jebrail, G. Ray, M. G.-E. Chauleau, P. M. Lundquist, A. Tocigl, J. P. Cannistraro, G. Scott, S. Seiler, R. Lal, E. Carvajal, E. Cervantes, N. Sergeev, Y.-H. Chen, P. Kumar, F. Christodoulou, *WO/2019/046860*, **2019**.
- [22] R. Sista, Z. Hua, P. Thwar, A. Sudarsan, V. Srinivasan, A. Eckhardt, M. Pollack, V. Pamula, *Lab Chip* **2008**, *8*, 2091.
- [23] D. J. Boles, J. L. Benton, G. J. Siew, M. H. Levy, P. K. Thwar, M. A. Sandahl, J. L. Rouse, L. C. Perkins, A. P. Sudarsan, R. Jalili, V. K. Pamula, V. Srinivasan, R. B. Fair, P. B. Griffin, A. E. Eckhardt, M. G. Pollack, *Anal. Chem.* **2011**, *83*, 8439.

- [24] Y. Fan, X. Kong, D. Chai, B. Wei, Y. Zhang, *Micro Nano Lett.* **2020**, *15*, 163.
- [25] K. Mogi, S. Adachi, N. Takada, T. Inoue, T. Natsume, *Appl. Sci.* **2019**, *9*, 2406.
- [26] V. Soum, Y. Kim, S. Park, M. Chuong, S. Ryu, S. Lee, G. Tanev, J. Madsen, O.-S. Kwon, K. Shin, *Micromachines* **2019**, *10*, 109.
- [27] V. Pamula, M. Pollack, R. Fair, *US/2006/0194331A1*, **2006**.
- [28] M. G. Pollack, V. Srinivasan, V. K. Pamula, G. Brackett, K. R. Brafford, D. Clark, Z. Hua, S. Norton, R. Sista, G. F. Smith, R. A. Sturmer, A. Sudarsan, P. Thwar, T.-H. Wang, T. Winger, *WO/2011/002957A2*, **2011**.
- [29] M. Abdelgawad, S. L. S. Freire, H. Yang, A. R. Wheeler, *Lab Chip* **2008**, *8*, 672.
- [30] Jian Gong, Chang-Jin Kim, in *18th IEEE Int. Conf. on Micro Electro Mechanical Systems*, IEEE, Piscataway, NJ **2005**, pp. 726–729.
- [31] Jian Gong, Chang-Jin Kim, *J. Microelectromech. Syst.* **2008**, *17*, 257.
- [32] R. Fobel, A. E. Kirby, A. H. C. C. Ng, R. R. Farnood, A. R. Wheeler, *Adv. Mater.* **2014**, *26*, 2838.
- [33] G. Sathyanarayanan, M. Haapala, C. Dixon, A. R. Wheeler, T. M. Sikanen, *Adv. Mater. Technol.* **2020**, *5*, 2000451.
- [34] H. Ko, J. Lee, Y. Kim, B. Lee, C.-H. Jung, J.-H. Choi, O.-S. Kwon, K. Shin, *Adv. Mater.* **2014**, *26*, 2335.
- [35] N. Ruecha, J. Lee, H. Chae, H. Cheong, V. Soum, P. Preechakasedkit, O. Chailapakul, G. Tanev, J. Madsen, N. Rodthongkum, O.-S. Kwon, K. Shin, *Adv. Mater. Technol.* **2017**, *2*, 1600267.
- [36] R. Fobel, C. Fobel, A. R. Wheeler, *Appl. Phys. Lett.* **2013**, *102*, 193513.
- [37] C. Degrand, A.-M. Martre, B. Limoges, B. Schöllhorn, *Analyst* **2001**, *126*, 887.
- [38] K. Tamaoku, K. Ueno, K. Akiura, Y. Ohkura, *Chem. Pharm. Bull.* **1982**, *30*, 2492.
- [39] A. A. Sklavounos, J. Lamanna, D. Modi, S. Gupta, A. Mariakakis, J. Callum, A. R. Wheeler, *Clin. Chem.* **2021**, in press, <https://doi.org/10.1093/clinchem/hvab180>.
- [40] T. Acharya, A. K. Ray, *Image Processing: Principles and Applications*, John Wiley & Sons, Inc., Hoboken, NJ, USA **2005**.